Ocean Engineering 125 (2016) 170–181

Contents lists available at ScienceDirect

Ocean Engineering

journal homepage: www.elsevier.com/locate/oceaneng

Study on docking guidance algorithm for hybrid underwater glider in currents

Canjun Yang [a], Shilin Peng [b], Shuangshuang Fan [c,*], Shaoyong Zhang [a], Pinfu Wang [a], Ying Chen [a,d]

[a] The State Key Lab of Fluid Power Transmission and Control, Zhejiang University, Hangzhou 310027, China
[b] Institute of Electronics Information, Hangzhou Dianzi University, Hangzhou 310018, China
[c] College of Information Science and Electronic Engineering, Zhejiang University, Hangzhou 310027, China
[d] Ocean College, Zhejiang University, Hangzhou 316021, China

ARTICLE INFO

Article history:
Received 31 July 2015
Received in revised form
21 February 2016
Accepted 1 August 2016
Available online 23 August 2016

Keywords:
Hybrid underwater glider
Rotatable thruster
Docking
Guidance algorithm
Current

ABSTRACT

The development of a novel type of hybrid underwater glider (HUG) that combines the advantages of buoyancy-driven underwater glider and propeller-driven autonomous underwater vehicle (AUV) has recently received considerable interest. HUG is designed with a rotatable thruster to ensure the enough maneuverability of the vehicle for underwater docking. Unlike the fixed funnel-type dock, the dock proposed here can rotate actively to allow the vehicle to approach the docking station from most range of directions providing better accessibility for the vehicle. Considering that the ocean current may have a significant impact on the HUG, a pursuit guidance algorithm with current compensation is presented. The performance of the guidance algorithm is compared with other existing guidance algorithms, such as pure pursuit guidance and proportional navigation guidance by simulation based on the dynamic model of HUG. Moreover, underwater docking experiments are conducted to validate the feasibility of the docking system and the effectiveness of the proposed guidance algorithm. The experimental results indicate that the proposed algorithm compensates well for the current disturbances on HUG docking mission and the HUG can dock with the rotatable dock entrance successfully.

1. Introduction

Underwater gliders are highly efficient, winged underwater vehicles that propel themselves by modulating their buoyancy and attitude (Mahmoudian and Woolsey, 2008). These gliders are widely used in oceanographic research because of their low cost, long range, and high endurance. However, the low-speed capability presents with significant problems when operating in areas with strong water currents that exceed the glider's maximum forward speed (Claus et al., 2010). Moreover, gliders have limited applications because they do not have horizontal flight capabilities. By contrast, conventional propeller-driven autonomous underwater vehicles (AUVs) have high maneuverability, but their endurance time usually ranges from hours to days, which is much less than underwater gliders.

A novel type of hybrid underwater glider (HUG) that combines the advantages and features of gliders and AUVs is proposed (Bachmayer et al., 2004; Jenkins et al., 2003). Several types of HUG have already been developed in previous studies. Alvarez et al. (2009) and Caffaz et al. (2010) fabricated a HUG called Folaga. Claus et al. (2010) developed a low-power, propeller-based propulsion module to augment the buoyancy engine of a 200 m Slocum electric glider. Wang et al. (2010, 2011) developed a HUG called PETREL. Isa and Arshad (2013) and Isa et al. (2014) presented a mathematical model and analysis of the motion control for a USM (Universiti Sains Malaysia) hybrid-driven underwater glider, which has independently controllable wings and a rudder. A concept of a gliding robotic fish that combines gliding and fin-actuation mechanisms has also been presented (Feitian et al., 2014; Tan, 2011; Zhang et al., 2012). However, few studies have considered a HUG with docking capability. If a HUG can dock with an underwater station with enough maneuverability for battery recharging and data communication, vehicle endurance can be enhanced a lot. We can then expand glider applications, for example, oceanographic scientists who aim to monitor long-term change of the ocean, can benefit from the long-term deployment of HUGs instead of recovering the vehicles and replacing the batteries after each mission. Furthermore, if the docking station is connected to a cabled ocean observatory (Chen et al., 2012a, 2012b, 2013), the HUGs can be considered as additional mobile

* Corresponding author.
E-mail addresses: ssfan@zju.edu.cn, fanshuangshuang@163.com (S. Fan).

http://dx.doi.org/10.1016/j.oceaneng.2016.08.002
0029-8018/

nodes for three-dimensional ocean observation. Considering the benefits described above, Zhejiang University is developing a HUG for underwater docking (Peng et al., 2014). In this paper, a small-scaled hybrid underwater glider called Mini-HUG, is developed for the validation of docking scheme and guidance algorithm, considering its convenience for deployment and operation. For a vehicle to perform underwater docking, horizontal flight capability and high maneuverability are obviously necessary, which are two important features of the vehicle to realize underwater docking. Typically, underwater gliders are driven by a buoyancy engine and do not have horizontal flight capability to perform underwater docking. Moreover, the low maneuverability of underwater gliders also adds the challenge for potential docking. Therefore, for underwater gliders, docking is a more difficult and possibly different problem. In our case, by the concept of 'hybrid', the HUG has horizontal flight capability. However, given the low speed of our HUG, a key technical challenge in vehicle design is how to obtain high maneuverability at low speeds for underwater docking (Peng et al., 2013). As conventional AUVs use control fins to control the yaw and pitch, and their steering capability is strongly coupled with their velocities, they have to reach a minimum speed to maintain control authority and counteract the positive buoyancy (Morel, 2002; Woolsey, 2005). Although the minimum speed may differ depending on vehicle configuration, Thivierge et al. (2005) showed that most control fins are effective as long as the vehicle's velocity is 1 m/s (two knots) or faster. Given that the speed of our glider is low, the traditional fin-steering method is unsuitable for our case. We thus attempt to design a HUG whose yaw is controlled by the rotation of the thruster and whose pitch is controlled by a longitudinal moving mass.

In terms of the dock, there are two most common dock designs for flying vehicles: one is a pole type (Singh et al., 2001); another is a funnel type (Allen et al., 2006; McEwen et al., 2008; Park et al., 2009). As we will discuss latter, each type has its own pros and cons. To integrate the advantages of both types, this paper introduces a rotatable funnel-shaped dock, which can rotate around its vertical axis actively. The dock proposed here can rotate actively to allow the vehicle to approach the docking station from most range of directions providing better accessibility for the vehicle, thus reducing the complexity of the docking algorithm.

With regard to the underwater docking, the docking guidance algorithms are of vital importance. McEwen et al. (2008) presented a cross-track-error based docking control algorithm for a unidirectional docking system. Park et al. (2009) introduced a vision-guidance docking algorithm with PID controllers for the vertical and horizontal plane. Kim (2007) derived a linear terminal guidance (LTG) controller in the framework of optimal control for AUV docking. Because the LTG controller does not consider the effect of ocean currents, a modified LTG is addressed by Park et al. (2011a, 2011b) for unidirectional docking compensating the effect of currents. Teo et al. (2012, 2015) gave a fuzzy docking guidance that can handle unknown currents. However, few studies have been conducted on the docking algorithms of funnel-shaped rotatable docking system. This paper aims to develop a docking guidance algorithm for the rotatable docking system; the effect of ocean currents is also taken into consideration.

The paper is organized as follows. Section 2 presents the details of the docking system developed by Zhejiang University. A novel type of HUG with a rotatable thruster is first proposed. Since HUG is an underactuated vehicle, an underwater station with a rotatable dock entrance is designed to assist the vehicle for docking. In Section 3, the dynamic model of HUG is derived briefly, which is the basis of numerical simulation for motion prediction and algorithm validation. Considering that the ocean current may have a significant impact on the motion of HUG, a pursuit guidance algorithm with current compensation is proposed in Section 4, whose performance is compared with the existing guidance algorithm by simulation. Section 5 gives the results of underwater docking experiments which are conducted to validate the feasibility of the docking system and the effectiveness of the proposed guidance algorithm. Section 6 summarizes the main contributions and describes some additional avenues for continuing research.

2. Docking system

For long-term sustainability, an AUV or HUG should be able to autonomously perform its mission and dock at a deployed underwater docking station for data downloads, battery recharging, and new mission script upload for the next mission operation. According to the functions of the docking system, it can be divided into three main parts: the autonomous vehicle, which is a HUG in our case; the mechanical system of a docking station with navigation and guidance accessories, such as the acoustic transducer and the light source, and so on; and the power and data transmission system. More details on our docking system are presented as follows.

2.1. Hybrid underwater glider

A small-scaled hybrid underwater glider called Mini-HUG, is developed for the validation of the docking scheme and guidance algorithm, motivated by its convenience for deployment and operation. The main specifications of Mini-HUG are shown in Table 1. For a vehicle to perform underwater docking, horizontal flight capability and high maneuverability are obviously necessary, which are two important features of the vehicle to realize underwater docking. Given the low speed of our HUG, a key technical challenge in vehicle design is how to obtain high maneuverability at low speeds for underwater docking. Due to this, a rotatable thruster and a longitudinal moving mass are adopted to control the yaw and the pitch movements, respectively.

2.1.1. Mini-HUG design overview

As shown in Fig. 1, Mini-HUG can be divided into four sections: Bow Section, Main Section, Electronic Section, and Thruster Section. Specifically, the Bow Section is a flood section, which holds a camera and the flooding part of the ballast system. The Main Section contains the attitude control system and the sealed part of the ballast system. The attitude control system regulates the pitch angles of the vehicle by moving an internal mass. The ballast system changes the net weight of the vehicle by pumping water inside or outside the vehicle. The Main Section also contains the control and signal processing boards, the navigation devices as well as the battery. The GPS and communication terminals together with the antennas are all fixed in the Electronic Section. In the Thruster Section, there is a thruster which can rotate around

Table 1
Main specifications of Mini-HUG.

Feature	Description
Length	1 m
Diameter	130 mm
Weight in air	7.85 kg
Operating depth	0 ~ 10 m
Deflection angle of thruster	±45°
Ballast system	Piston-cylinder
Communications	Radio
Sensors	TCM5, depth sensor, camera, GPS receiver
Battery	Lithium battery
Operating in glider mode	0.2–0.4 m/s
Operating in AUV mode	0.2–0.6 m/s

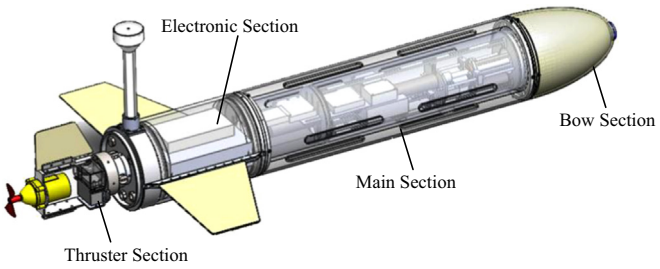

Fig. 1. Configuration of hybrid underwater glider.

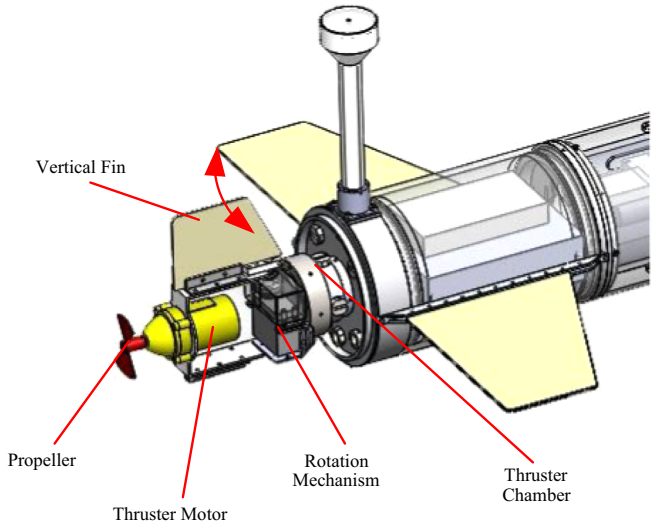

Fig. 2. The rotatable thruster of Mini-HUG.

its vertical axis, which acts as a rudder as well.

The rotatable thruster is designed with special consideration to increase the turning (or heading) maneuverability of the vehicle. It consists of a thruster chamber, a rotation mechanism, a thruster motor, a propeller, and a vertical fin; see Fig. 2. The rotation mechanism with a steering engine is used to swing the thruster to control the vehicle heading. When the steering engine works causing the thruster motor, the propeller, and the vertical fin together to have a deflection angle around its vertical axis. This yields dual steering effects: the thruster with a deflected angle generates a turning torque, while the swung vertical fin has the heading effect as a regular rudder.

2.1.2. Turning capability validation

The HUG with a rotatable thruster has higher maneuverability even at low speeds compared with conventional AUV which uses control fins to turn. To validate this improvement, a series of turning experiments have been carried out comparing two different types of HUG configurations. The difference between the two types of configurations is that for one, HUG uses conventional rudder to turn; while for another, HUG adopts rotatable thruster to turn.

During the turning tests, the deflection angles of the rudder or the rotatable thruster (as well as the vertical fin) was set to be 45°, 40°, 35°, and 30°, respectively. Table 2 gives the turning diameters for the two types of configurations. As noted in the table, the turning diameters of the HUG with rotatable thruster are significantly smaller than that of the HUG with a conventional rudder. The experimental tests indicate that the HUG with a rotatable thruster can provide higher maneuverability than conventional HUGs and AUVs that use control fins to steer; and this type of configuration is more suitable for the low-speed HUG to implement underwater docking.

Table 2
Turning diameters for different turning configurations.

HUG with conventional rudder configuration		HUG with rotatable thruster configuration	
Rudder deflection angle (°)	Turning diameter (m)	Thruster deflection angle (°)	Turning diameter (m)
45	8.4	45	1.1
40	8.6	40	3.0
35	9.6	35	3.0
30	10.4	30	4.3

2.2. Dock station overview

The most common dock designs for flying vehicles, which rely on sustained forward motion for control, are a pole type and a funnel type (McEwen et al., 2008). The pole-type dock is omnidirectional and can be approached from any direction (Kim, 2007). This eases the constraint on heading control, but the mechanical implementation of the docking system may be more complicated and offers less vehicle protection (Kim, 2007). The funnel-type dock has a cone shape entry, which is used to channel the vehicle into a tube where it is captured, and provides a simple dock design (McEwen et al., 2008). The funnel-type dock is typically fixed for its simplicity. However, the docking algorithms for the fixed funnel-type dock may be much complicated because it can only be approached from a fixed direction. Another kind of funnel-type dock, which is similar to a weathervane, is omnidirectional, providing better accessibility for the docking vehicle. However, this design has to transfer power and data across a moving interface, most likely using a slip ring, which brings additional complexity to the mechanical structure (McEwen et al., 2008).

Considering that the funnel-type dock is simpler and can provide better vehicle protection (McEwen et al., 2008), we choose the rotatable funnel-type dock for our design, whose dock entrance can rotate around the dock vertical axis actively. However, unlike the weathervaning cone, the rotatable dock is not omnidirectional, and the limitation of the rotation angle is due to the length of the power and communication cables, such as the one which connects the underwater lamp fixed on the rotatable funnel of the dock with the sealed electronic cabin fixed on the support of the dock and provides power for the underwater lamp; see Fig. 3. Therefore, the rotating range of dock is about $[-120^{\circ}, 120^{\circ}]$ in our design. In this case, a slip ring is not necessary, while the rotatable dock can decrease the difficulty of HUG docking control. Fig. 3 shows the docking system with a rotatable dock entrance. When the vehicle approaches the dock, it transmits its heading angle to the dock station. The dock then rotates the entrance to follow the vehicle's heading accordingly.

2.3. Power and data transmission system

The power connection is achieved by an inductive link, with one inductive coil on the vehicle and a corresponding coil on the docking station. High-speed data communication with the dock is achieved by a wireless network link through WiFi antennas. Although the range for WiFi connection is limited in water, our experiments indicate that high-speed data transmission can still be achieved if the gap in seawater between the WiFi antennas is less than 55 mm (Shi et al., 2012). In our case, when the vehicle enters the docking tube, the seawater gap is less than 30 mm to maintain reliable data transmission. The debugging and testing of these

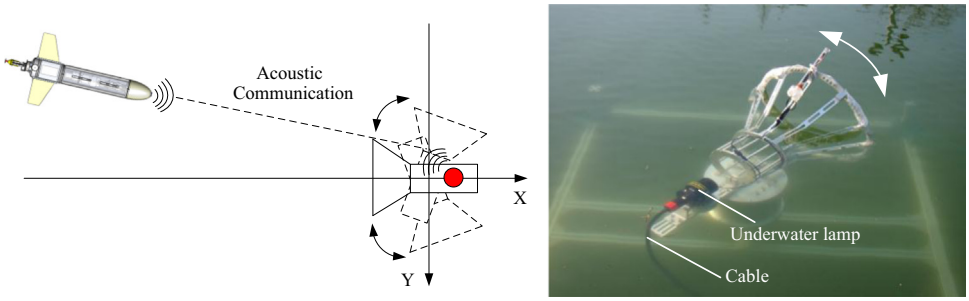

Fig. 3. Docking scheme with a rotatable dock.

components for docking are in process.

3. Dynamic model in currents

The dynamics of a HUG with a rotatable thruster has been fully derived in Peng et al. (2014). In order to illustrate the following guidance algorithm, we further consider the effect of currents here and derive vehicle dynamics in currents, which will be used for numerical simulations in Section 4.

The multi-body Mini-HUG is modeled as a rigid body (mass m_{rb}) with a single moving point mass m_p which can move longitudinally along the vehicle's centerline for the pitch adjustment of the vehicle, as well as a rotatable thruster for the yaw adjustment. The HUG also includes a variable ballast actuator, which is modeled as a fixed-position variable point mass (m_b). The total vehicle mass is

$$m = m_{rb} + m_p + m_b$$

The vehicle displaces a fixed volume of fluid of mass $\overline{m}$ so that the net weight can be described as

$$W = mg - \overline{m}g$$

3.1. Kinematics

Define a body-fixed, orthonormal reference frame centered at the center of buoyancy (CB) of the vehicle and represented by the unit vectors $\boldsymbol{b}_1$, $\boldsymbol{b}_2$ and $\boldsymbol{b}_3$. The vector $\boldsymbol{b}_1$ is aligned with the longitudinal axis of the vehicle, $\boldsymbol{b}_2$ points out the right wing, and $\boldsymbol{b}_3$ completes the right-handed triad; see Fig. 4. Define another orthonormal reference frame, denoted by the unit vectors $\boldsymbol{i}_1$, $\boldsymbol{i}_2$, and $\boldsymbol{i}_3$, which is fixed in inertial space such that $\boldsymbol{i}_3$ is aligned with the force due to gravity. Let $\boldsymbol{X} = [x, y, z]^T$ represent the position vector from the origin of the inertially fixed frame to the origin of the body-fixed frame, which is expressed in the inertial frame. The orientation of the vehicle is given by the rotation matrix $\boldsymbol{R}_{IB}$, which is parameterized by Euler angles, that is: the roll angle φ, the pitch angle θ and the yaw angle ψ. $\boldsymbol{R}_{IB}$ can map free vectors from the body-fixed frame to the inertially fixed frame (Fossen, 1995). Let

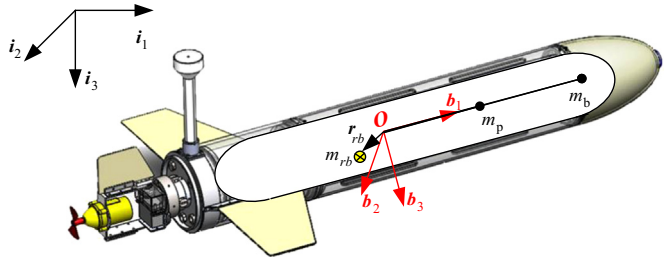

Fig. 4. Illustration of reference frames.

$\boldsymbol{v} = [u, v, w]^T$ and $\boldsymbol{\omega} = [p, q, r]^T$ represent the translational and rotational velocity of the vehicle with respect to the inertial frame, but expressed in the body-fixed frame.

The current velocity described in the inertial frame is

$$\boldsymbol{V}_f = \begin{pmatrix} V_{fx} \\ V_{fy} \\ V_{fz} \end{pmatrix}$$

Since it is common to derive vehicle dynamics in the body-fixed frame, current velocity with respect to inertial frame described in the body-fixed frame is like this

$$\boldsymbol{v}_f = \begin{pmatrix} u_f \\ v_f \\ w_f \end{pmatrix} = R_{IB}^T V_f$$

Thus, the vehicle velocity relative to the current is

$$\boldsymbol{v}_r = v - \boldsymbol{v}_f$$

The kinematic equations (Graver, 2005; Mahmoudian, 2009) are

$$\dot{\boldsymbol{X}} = \boldsymbol{R}_{IB}\boldsymbol{v} \tag{1}$$

$$\dot{\boldsymbol{R}}_{IB} = \boldsymbol{R}_{IB}\hat{\boldsymbol{\omega}} \tag{2}$$

where $\hat{}$ denotes the 3×3 skew-symmetric matrix satisfying $\hat{\boldsymbol{a}}\boldsymbol{b} = \boldsymbol{a} \times \boldsymbol{b}$ for vectors $\boldsymbol{a}$ and $\boldsymbol{b}$.

The kinematic equations of vehicle in currents has no difference from the ones without currents. One should note that the total velocity of the vehicle includes the component of current relative velocity and the current velocity.

In addition to the six degrees of freedom associated with the vehicle's translation and rotation, there is one degree of freedom associated with the moving mass m_p, which is modeled as a particle moving along $\boldsymbol{b}_1$ and used for pitch angle regulation. Let $\boldsymbol{r}_p = [r_{px}, 0, 0]^T$ represent the position of m_p relative to the origin of the body-fixed frame. Thus, the kinematic equation of the moving mass is

$$\boldsymbol{v}_p = \boldsymbol{v} + \boldsymbol{\omega} \times \boldsymbol{r}_p + \dot{\boldsymbol{r}}_p \tag{3}$$

Eqs. (1)–(3) describe the kinematics of the entire vehicle system.

3.2. Dynamics

Let $\boldsymbol{\eta}$ denote the generalized velocity of the vehicle and let $\boldsymbol{\eta}_f$ represent the generalized flow velocity in dimensions consistent with $\boldsymbol{\eta}$

$$\boldsymbol{\eta} = \begin{pmatrix} \boldsymbol{v} \\ \boldsymbol{\omega} \\ \dot{r}_{px} \end{pmatrix} \tag{4}$$

$$\boldsymbol{\eta}_{\mathrm{f}} = \begin{pmatrix} \boldsymbol{v}_{\mathrm{f}} \\ \boldsymbol{0} \\ 0 \end{pmatrix} \tag{5}$$

The generalized velocity relative to the flow is

$$\boldsymbol{\eta}_{\mathrm{r}} = \boldsymbol{\eta} - \boldsymbol{\eta}_{\mathrm{f}} = \begin{pmatrix} \boldsymbol{v}_{\mathrm{r}} \\ \boldsymbol{\omega} \\ \dot{r}_{\mathrm{px}} \end{pmatrix} \tag{6}$$

Here, in order to avoid the complexity of re-deriving the full dynamics of HUG in currents, we refer to the existing study of Woolsey (2011) and Fan and Woolsey (2014), and assume that the vehicle is neutrally buoyancy, the vehicle's center of mass (CM) coincides with the CB, and the flow is uniform, thus the flow-relative dynamic model can be written as this

$$\mathbb{M}\dot{\boldsymbol{\eta}}_{\mathrm{r}} = -\begin{pmatrix} \hat{\boldsymbol{\omega}} & \boldsymbol{0} & \boldsymbol{0} \\ \hat{\boldsymbol{v}}_{\mathrm{r}} & \hat{\boldsymbol{\omega}} & \boldsymbol{0} \\ \boldsymbol{0} & \boldsymbol{0} & 0 \end{pmatrix}\mathbb{M}\boldsymbol{\eta}_{\mathrm{r}} - \mathbb{M}\dot{\boldsymbol{\eta}}_{\mathrm{r}} + \begin{pmatrix} \boldsymbol{0} \\ \boldsymbol{0} \\ \frac{1}{2}\boldsymbol{v}_{\mathrm{r}}^{T}\frac{\partial \mathbb{M}_{\mathrm{p}}(\boldsymbol{r}_{\mathrm{p}})}{\partial r_{\mathrm{px}}}\boldsymbol{v}_{\mathrm{r}} \end{pmatrix} + \begin{pmatrix} W\boldsymbol{\zeta} + \boldsymbol{f}_{\mathrm{v}} + \boldsymbol{f}_{\mathrm{prop}} \\ \boldsymbol{\tau}_{\mathrm{sys}} \\ m_{\mathrm{p}}g\boldsymbol{\zeta} + u_{\mathrm{px}} \end{pmatrix} \tag{7}$$

where $\mathbb{M}$ is the generalized inertia matrix of the vehicle system, including the generalized added inertia matrix; $\mathbb{M}_{\mathrm{p}}(\boldsymbol{r}_{\mathrm{p}})$ is the generalized inertia matrix for the moving particle; $\boldsymbol{\zeta} = \boldsymbol{R}_{\mathrm{lb}}^{T}\boldsymbol{i}_3$ is defined as the "tilt vector"; $\boldsymbol{\tau}_{\mathrm{sys}}$ is the external moments, $\boldsymbol{f}_{\mathrm{v}}$ denotes the viscous force acting on the vehicle, $\boldsymbol{f}_{\mathrm{prop}}$ is the propulsion force of the thruster, u_{px} is the input forces from the actuator that adjusts the HUG's pitch angle, all expressed in the body frame. One can find more details about the external forces and moments from Peng et al. (2014).

Dynamic Eq. (7) and Kinematic Eqs. (1)–(3) completely describe the motion and dynamics of the vehicle in currents.

4. Docking guidance algorithms

Actually there are similar docking problems in other domains, such as spacecraft rendezvous and docking, connection establishment during aerial refueling, and so on. However, since the control objects are different, the control difficulty is different. Compared with aircraft and airplane, AUV is a kind of under-actuated vehicle with low velocity and less maneuverability, which suffers from more serious ocean disturbances. Thus, special considerations should be taken for underwater docking problem. Most of all, the powerful docking guidance algorithms are the key to ensure successful underwater docking. In this section, the docking problem is firstly described mathematically and the docking scheme adopted is overviewed. Considering that the ocean current may have a significant impact on the HUG, a pursuit guidance algorithm with current compensation is proposed, whose performance is compared with other guidance algorithms, such as pure pursuit guidance and proportional navigation guidance by simulation.

As for the current measurement, there is normally no ADCP onboard a small glider or HUG, and this presents problems for underwater docking in currents. In practice, an Acoustic Doppler Current Profilers (ADCP), which is used to measure the current, is equipped on the dock. The dock station gets the current information and sends it to the vehicle; the vehicle then uses this information in the guidance algorithm to compensate the current effect.

We assume that the depth of the docking station is known after deployment. Then the docking motion control can be decoupled into two parts: the depth control in the vertical plane and the motion control in the horizontal plane. Since the depth control problem in underwater docking is the same to that in the depth-keeping cruising problem, which is well studied in many literatures (Claus et al., 2012; Hu et al., 2013; Watson and Green, 2014), this paper will focus on the docking algorithms in the horizontal plane.

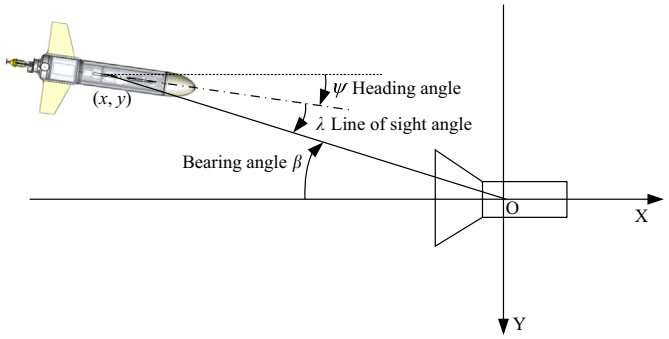

Fig. 5. Coordinate system of docking.

4.1. Coordinate system

Referring to Kim (2007), the coordinate system of docking in the horizontal plane is defined in Fig. 5. To simplify the problems without loss of generality, the funnel-type dock is assumed to be located at the origin of the inertia frame. The position of the vehicle is (x, y) in the inertia frame. β is the bearing angle which is defined from the centerline of the dock to the line between the origin of the inertia frame and the vehicle position; ψ is the heading angle of the vehicle with respect to the x-axis of docking frame. In addition, λ is defined as the line-of-sight angle from the centerline of the vehicle to the line between the vehicle and the origin of inertia frame. According to Fig. 5, it is not hard to figure out the relationship among these three angles:

$$\beta = \psi + \lambda \tag{8}$$

4.2. Mathematical problem of docking

In order to evaluate the guidance performance of the docking control algorithm, it is necessary to describe the docking problem mathematically. The cone-shape entry of the funnel-type dock can be assumed as a triangle PAB in the horizontal plane, as is shown in Fig. 6, where PA and PB denote the outline of the cone-shape entry, R_{d} is the maximum radius of the cone-shape entry, ε is the angle between the sides PA and AB. The moment when the vehicle nose arrived at the cone-shape entry is defined as t_{f}. The heading angle and the lateral position deviations of the vehicle nose with respect to the dock centerline are denoted respectively by $\Delta\psi_{\mathrm{f}}$ and Δy_{f} at the time of t_{f}. Thus, one of the basic requirements for the successful docking is $|\Delta y_{\mathrm{f}}|$ less than R_{d}. Besides, since the cone-shape entry of the dock has the function of channeling the vehicle to enter the tube behind, the channeling effect will be active if $|\Delta\psi_{\mathrm{f}}|$ less than ε.

Based on the above statements, the docking problem can be described as this: under the effective navigation and guidance algorithm, the vehicle can enter the dock entrance with the final states like this:

$$\begin{cases} |\Delta\psi_{\mathrm{f}}| < \varepsilon - \varepsilon' \\ |\Delta y_{\mathrm{f}}| < R_{\mathrm{d}} - R_{\mathrm{d}}' \end{cases} \tag{9}$$

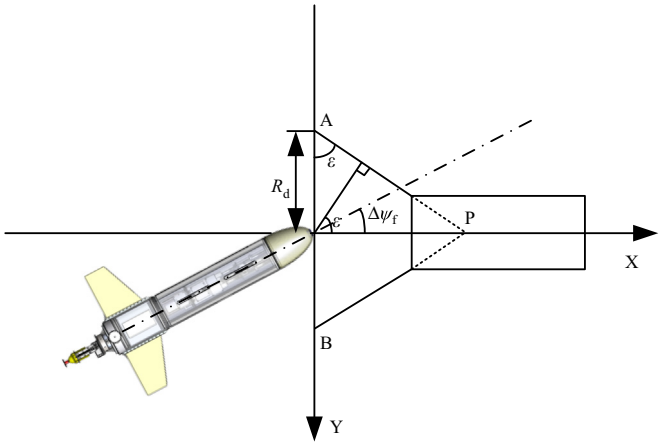

Fig. 6. Docking problem for directional docks.

Table 3
Docking specifications and requirements.

Variable	Value
R_d	0.55 m
R_d'	0.05 m
ε	60°
ε'	15°
$\lvert\Delta\psi_f\rvert$	45°
$\lvert\Delta y_f\rvert$	0.5 m

where ε' and R_d' are the safety margins for successful docking. Table 3 lists the specifications of our docking station and the corresponding docking control requirements.

With regard to the docking problem for a rotatable dock, we assume that the dock can follow the vehicle's heading accurately so that $\Delta\psi_f = 0$ (Fig. 7). In the light of the assumption, the successful docking requirement is simplified as:

$$\lvert\Delta y_f\rvert < R_d - R_d' \tag{10}$$

Therefore, in the following simulation, the docking station is described as a yellow point, which shows the acceptable docking area for successful docking attempt; see the yellow point in Fig. 7, the radius of which is equal to $R_d - R_d'$. If the HUG can arrive at the area within the yellow point, the vehicle will enter the dock entrance successfully; otherwise, the vehicle will fail to enter the dock entrance.

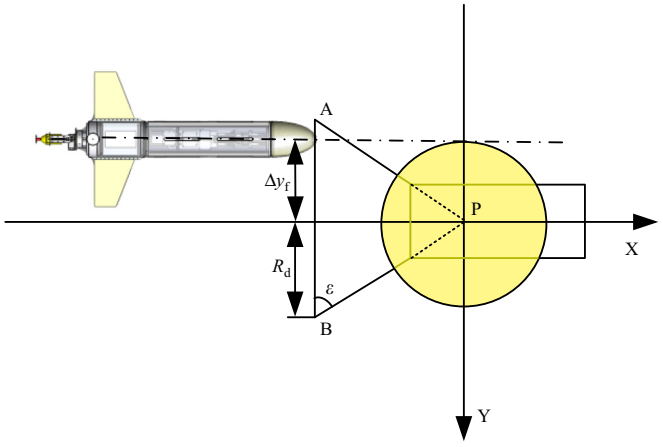

Fig. 7. Docking problem for a rotatable dock ($\Delta\psi_f = 0$).

4.3. Navigation strategy for docking

The navigation strategy for docking depends on the navigation and positioning devices. Comparing the performance of different devices, we choose ultrashort base line (USBL) and camera for docking control. Assuming the 3D (3 degrees of freedom) position of the dock is known ahead, the HUG approaches the dock with the dead-reckoning devices at the beginning of the dock process. Once the USBL bearing is obtained, the docking program is started. As the distance between the dock and the vehicle varies, also according to the performance limits of the navigation and positioning devices, the docking process is divided into three sequences: long-distance homing stage, medium-distance adjustment stage, and the proximal docking stage.

In the long-distance homing stage, the vehicle keeps tracking the USBL signals from the dock for increasing signal strength; in the meanwhile, the vehicle is controlled to reach the same depth as the dock located. In the medium-distance adjustment stage, the USBL bearing and fix are obtained, with which the vehicle is controlled to reduce the heading and cross-track derivations with respect to the centerline of the dock. The proximal docking stage begins when the vehicle is 15 m far away from the dock, since the vision navigation information can be computed from the camera image at this range. This final stage is key to the whole docking process, so both the USBL and vision information are adopted for navigation and control. As for the dock with fixed entrance, both the heading and cross-track deviations should be decreased as far as possible. For the dock with rotatable entrance, the dock entrance starts to rotate after the proximal docking stage begins, trying to follow the vehicle's heading, so the vehicle is only required to arrive at the dock position as exact as possible. In this paper, we focus on the study of guidance algorithms on the proximal docking stage for a rotatable dock as follows.

4.4. Pure pursuit docking guidance

4.4.1. Algorithm description

With the current positioning information, pure pursuit guidance algorithm calculates the desired heading angle aiming to keep the vehicle pointing to the dock station. Fig. 8 shows the principle of the pure pursuit guidance algorithm. The desired heading angle can be solved as this:

$$\psi_d = \beta = \arctan\frac{y}{x}$$

The calculated heading angle is used for heading control. As is shown in Fig. 9, the pure pursuit guidance algorithm determines the desired heading angle ψ_d, which is the input of the heading controller. The heading controller makes the vehicle follow the desired heading angle with feedback control. When the actual heading angle of the vehicle equals to the desired heading angle, the vehicle can point to the docking station exactly.

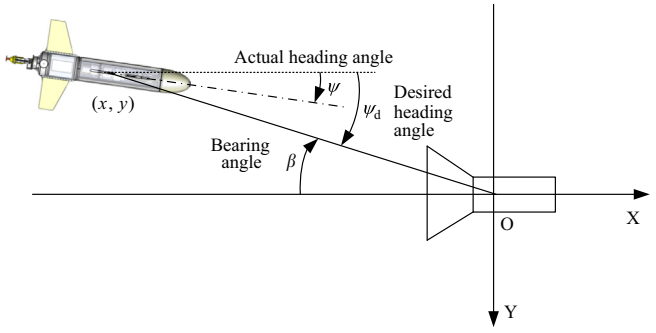

Fig. 8. Principle of the pure pursuit guidance algorithm.

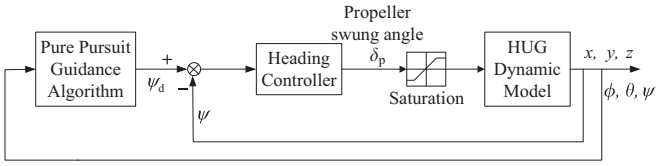

Fig. 9. Block diagram of pure pursuit guidance algorithm.

Because the range of the arc tangent operation is $[-\pi/2, \pi/2]$, the desired heading angle should be modified according to the vehicle's quadrant. The desired heading angle after modification is:

$$\psi_d = \beta = \begin{cases} \arctan\frac{y}{x} & x < 0 \\ \pi + \arctan\frac{y}{x} & x > 0 \\ \frac{\pi}{2} & x = 0,\ y < = 0 \\ \frac{3\pi}{2} & x = 0,\ y > 0 \end{cases} \tag{11}$$

4.4.2. Simulation results

The pure pursuit guidance algorithm is easy to achieve and guides the vehicle towards the dock ensuring that the dock is always in the view of the USBL and the camera. Fig. 10 shows the simulation results of the pure pursuit guidance algorithm without current disturbance. Since the final stage of docking mission determines the success or failure of docking attempt, here we take this stage into consideration to verify the effectiveness of the guidance algorithm. The dock is located at the origin of the inertia frame; the vehicle starts from the same line $x = -15$ with different cross-track deviations, respectively, with the same heading angle $\psi = 0^\circ$; the speed of the vehicle is 0.5 m/s. The simulation results indicate that the pure pursuit guidance algorithm has the desired effect on the docking motion if the ocean currents are absent. The vehicle can approach the entrance successfully with different initial cross-track deviations. Since the dock entrance can rotate to follow the vehicle, there is a less strict requirement on the vehicle heading for the final docking progress.

Fig. 11 presents the docking trajectory of HUG under pure pursuit guidance in cross currents, the vehicle starts from the same point of $(-15, 0)$ with the same heading angle $\psi = 0^\circ$ under different current disturbances. The speed of the vehicle is 0.5 m/s. It can be found that the cross currents have remarkable effects on the docking motion of the vehicle. As the velocity of the current V_{fy} increases, the cross-track deviation of the vehicle with respect to the centerline of the dock grows. The pure pursuit guidance algorithm has no compensation on the current effects, the currents with increasing velocity may cause the failure of docking attempt, which occurs when V_{fy} equals to $\pm$ 0.2 m/s in the simulation.

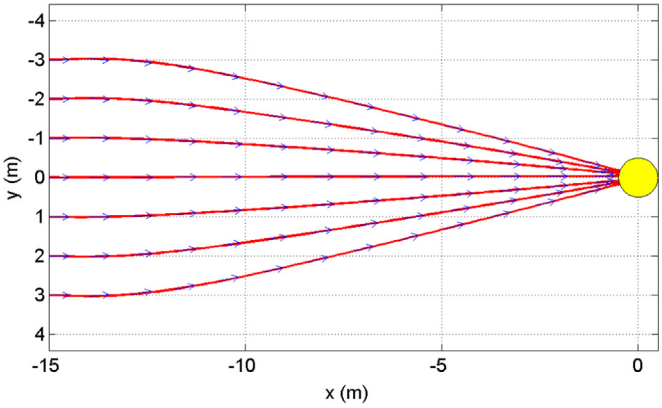

Fig. 10. Docking trajectory of HUG under pure pursuit guidance without currents. The blue arrows indicate the heading of vehicle; the yellow point shows the acceptable docking area for successful docking attempt. (For interpretation of the references to color in this figure legend, the reader is referred to the web version of this article.)

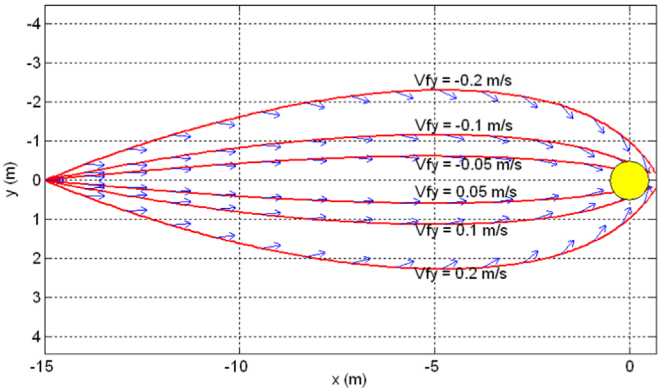

Fig. 11. Docking trajectory of HUG under pure pursuit guidance in cross currents. The blue arrows indicate the heading of vehicle; the yellow point shows the acceptable docking area for successful docking attempt. (For interpretation of the references to color in this figure legend, the reader is referred to the web version of this article.)

4.5. Proportional navigation guidance

4.5.1. Algorithm description

The optimal control is widely applied in many fields, such as the space, air, etc. (Cottrell, 1971; Ryoo et al., 2006; Shaferman and Shima, 2008; Steinfeldt et al., 2010; Xu and Liang, 2015). In the field of underwater docking, Kim (2007) described a terminal controller design procedure under the framework of optimal control. In his research, the proportional navigation guidance (PNG) algorithm is derived as an optimal terminal controller for a specific setting. The PNG algorithm, which is widely used for the terminal guidance of missile interception, can be also applied to the docking guidance of vehicles. In this paper, the PNG algorithm considering the effect of ocean currents is discussed. According to (Kim, 2007), the PNG law is given by:

$$r^* = 3\dot{\beta} \tag{12}$$

where r^* is the optimal heading rate command.

The bearing angle can be provided by

$$\tan\beta = \frac{y}{x} \tag{13}$$

Differentiating Eq. (13) and substituted by the kinematic equations, gives

$$\dot{\beta} = \frac{x\dot{y} - y\dot{x}}{(x^2 + y^2)} = \frac{x(V_0\sin\psi + V_{fy}) - y(V_0\cos\psi + V_{fx})}{(x^2 + y^2)} \tag{14}$$

So the PNG law in the coordinate system for docking can be given by

$$r^* = 3\dot{\beta} = 3 \times \frac{x(V_0\sin\psi + V_{fy}) - y(V_0\cos\psi + V_{fx})}{(x^2 + y^2)} \tag{15}$$

4.5.2. Simulation results

The simulation results of the PNG algorithm without current disturbance are shown in Fig. 12. The initial conditions of the dock and the vehicle for simulation are the same as the ones discussed

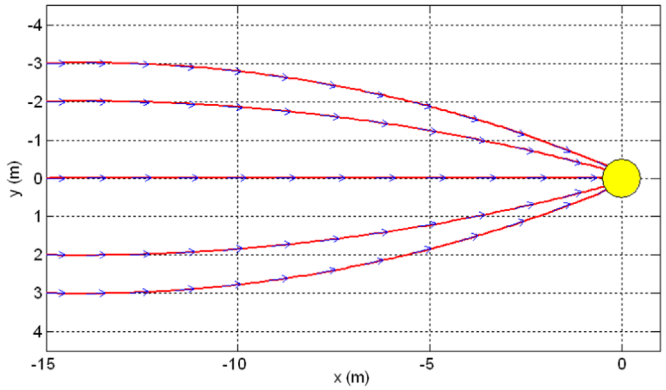

Fig. 12. Docking trajectory of HUG under proportional navigation guidance without currents. The blue arrows indicate the heading of vehicle; the yellow point shows the acceptable docking area for successful docking attempt. (For interpretation of the references to color in this figure legend, the reader is referred to the web version of this article.)

in Section 4.4.2. Similarly, the simulation results indicate that the PNG algorithm can guide the vehicle to the dock effectively with different initial cross-track deviations if there is no disturbance from the ocean currents.

If adding current disturbance with the flow velocity of $V_{fy} = 0.3$ m/s to the above simulations, we can investigate the effectiveness of the PNG algorithm under current disturbance. The simulation results are shown in Fig. 13. It can be found that the ocean currents still have some disturbance on the docking motion, but the PNG algorithm can compensate well for the current effects, the cross-track deviation can be reduced to the range required for successful docking. However, the PNG algorithm does not take the view range of the camera or USBL into consideration; the dock entrance is possible to be out of the view of the camera or USBL, which is equipped on the vehicle, during the docking process. Take point A on one of the simulated trajectories in Fig. 13 for example, the shadow region shows the view of camera when the vehicle passes through point A on the trajectory. We can find that the underwater lamp is outside the view of the camera at this moment, which means the vehicle loses the navigation information from the camera image at this point; this may cause a failure for the docking attempt.

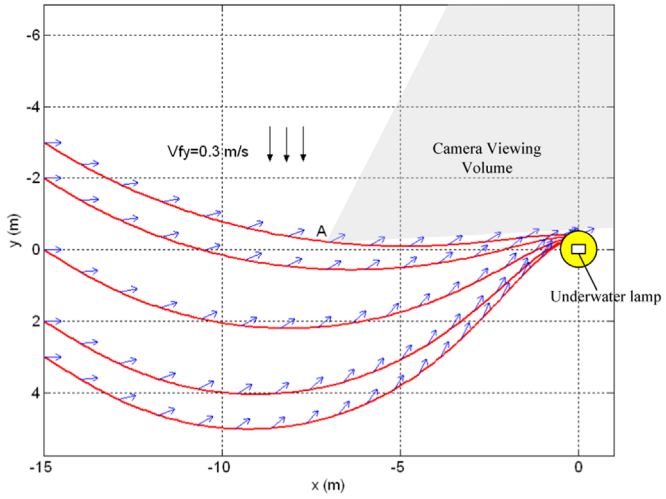

Fig. 13. Docking trajectory of HUG under proportional navigation guidance in cross currents. The blue arrows indicate the heading of vehicle; the yellow point shows the acceptable docking area for successful docking attempt; the rectangle in the origin indicates the underwater lamp. (For interpretation of the references to color in this figure legend, the reader is referred to the web version of this article.)

4.6. Pursuit guidance algorithm with current compensation

4.6.1. Algorithm description

Comparing the characteristics of the guidance algorithms discussed above, we see that the pure pursuit guidance algorithm keeps the vehicle pointing towards the dock, which ensures that the dock is within the view of the USBL or the camera throughout the docking mission; but the robustness of the algorithm is not satisfactory, which cannot compensate well for the current effect. As for the proportional navigation guidance algorithm, it has good capability to resist the disturbance of the ocean currents, but the dock may disappear from the view of the USBL or camera, since the line-of-sight angle is not taken into consideration in the algorithm.

Based on the above comparison, a novel guidance algorithm is proposed in this paper, which combines the advantages of the discussed algorithms. We call it pursuit guidance algorithm with current compensation. The principle of the algorithm is described as this: we choose a line-of-sight angle as the threshold in advance; during the flight, the vehicle computes the current line-of-sight angle with respect to the dock in real time; if the current line-of-sight angle is less than the threshold, a current compensation method is applied; if the current line-of-sight angle is greater than the threshold, we use the pure pursuit guidance algorithm to lock the target dock entrance and keeps the dock entrance in the view of the USBL or camera.

Referring to the way the plane lands in the presence of cross wind, that is the plane fly with a offset heading angle downstream the wind aiming to compensate the effects of the wind and make the flight trajectory coincide with the centerline of the runway (Crosswind landing, 2009), we present our guidance algorithm with current compensation here. Assuming that the lateral component of the current is V_{fy}, the corresponding compensation angle ψ_{crab} can be solved from this equation:

$$V_0 \sin \psi_{crab} = V_{fy}$$

We have

$$\psi_{crab} = \arcsin\frac{V_{fy}}{V_0}$$

In the actual operation, the computed compensation angle should be multiplied by a coefficient in order to avoid the appearance of an unreasonably large compensation angle, which may cause the dock lost in the view of the USBL or camera view. Since then, the actual compensation angle ψ_c is:

$$\psi_c = k_c \times \psi_{crab}$$

where k_c is the compensation coefficient. Then, the desired heading angle with current compensation is:

$$\psi_d' = \psi_d - \psi_c = \psi_d - k_c \times \arcsin\frac{V_{fy}}{V_0}$$

where ψ_d is the desired heading angle defined by Eqs. (11). Thus, the final desired heading angle which is determined by pursuit guidance with current compensation can be written as this:

$$\psi_d' = \begin{cases} \psi_d & \lambda > threshhold \\ \psi_d - k_c \times \arcsin\frac{V_{fy}}{V_0} & \lambda \le threshhold \end{cases} \quad (16)$$

In this algorithm, the tuning parameters are the line-of-sight angle threshold and the compensation coefficient k_c. The line-of-sight angle threshold decides when the current compensation is taken into account, which aims to keep the dock within the camera viewing volume. While the compensation coefficient k_c

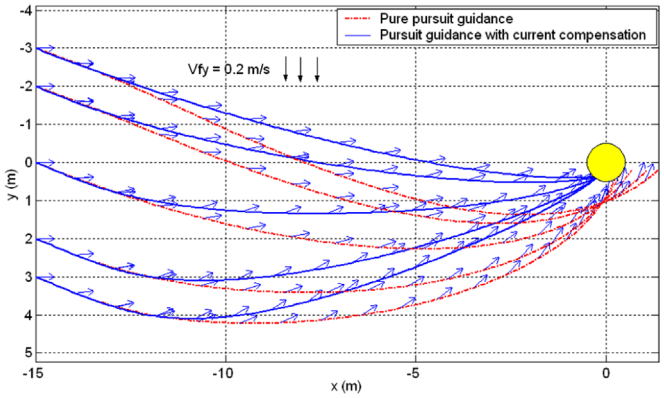

Fig. 14. Docking trajectories compared between pure pursuit guidance and pursuit guidance with current compensation. The blue arrows indicate the heading of vehicle; the yellow point shows the acceptable docking area for successful docking attempt. (For interpretation of the references to color in this figure legend, the reader is referred to the web version of this article.)

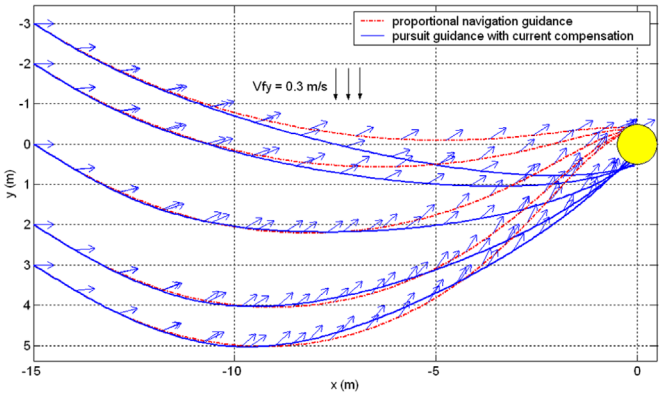

Fig. 16. Docking trajectory comparison between proportional navigation guidance and pursuit guidance with current compensation. The blue arrows indicate the heading of vehicle; the yellow point shows the acceptable docking area for successful docking attempt. (For interpretation of the references to color in this figure legend, the reader is referred to the web version of this article.)

determines the intensity of the current compensation. If k_c equals to 0, there is no current compensation. If k_c equals to 1, the effect of current is fully compensated. The compensation coefficient k_c is carefully tuned to make sure that the current is well compensated within the line-of-sight angle threshold.

4.6.2. Simulation results

The performance of the proposed pursuit guidance with current compensation is compared with the other two kinds of guidance algorithms by simulation. The initial conditions of the dock and the vehicle for simulation are the same as the ones discussed in Section 4.4.2. The compensation coefficient k_c of the pursuit guidance has the value of 0.5; the threshold of the line-of-sight angle is chosen as 18°.

Fig. 14 gives the docking trajectories comparison between pure pursuit guidance and pursuit guidance with current compensation. It can be seen that in the cross current with V_{fy} = 0.2 m/s, the vehicle under pure pursuit guidance algorithm may fail to enter the dock entrance, while the pursuit guidance algorithm with current compensation can lead the vehicle to dock with the entrance successfully. Line-of-sight angle of pursuit guidance with current compensation during docking process is shown in Fig. 15. It can be found that the line-of-sight angle maintains in the range of $[-30^\circ, +15^\circ]$ with HUG starts from different initial positions. As the field of view for the USBL and camera we apply are $\pm 60^\circ/\pm 35^\circ$ respectively, this indicates that the pursuit guidance algorithm with current compensation can keep the dock in the view of the USBL or camera.

Next, we compare the simulation results between proportional navigation guidance algorithm and pursuit guidance algorithm with current compensation. The initial condition and the parameters of the guidance algorithm are the same as the ones discussed above in this section. From Fig. 16, we see that the proportional navigation guidance algorithm can make the vehicle dock with the station successfully in the given cross current, but if moving to Fig. 17, it is obvious that the line-of-sight angle of proportional navigation guidance algorithm at the end of docking mission is larger than 35°, which indicates that the dock may be lost in the camera views of the vehicle, and may cause the failure of docking attempts.

Based on the discussion above, we can conclude that the performance of pursuit guidance algorithm with current compensation is superior to the other two ones, which takes both the view range of the sensors and the ocean current disturbance into account and ensures the success of docking attempt.

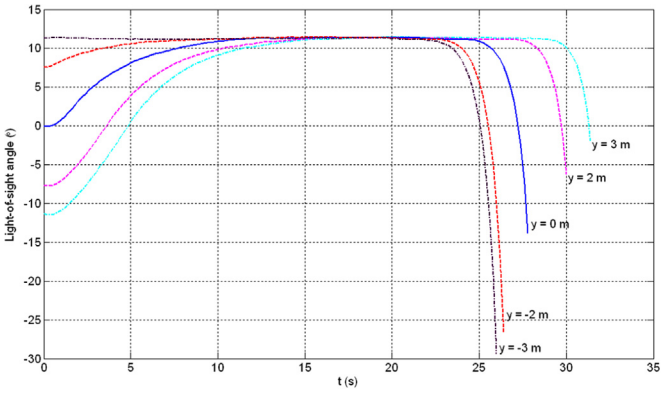

Fig. 15. Line-of-sight angle of pursuit guidance with current compensation during docking process.

5. Underwater docking experiments

The preliminary docking experiments in the swimming pool have been carried out to validate the performance of the proposed pursuit guidance algorithm with current compensation as well as the function of the docking system.

5.1. Docking system setup

In order to have an intuitive understanding of the docking process, the experiments were conducted on the surface of the

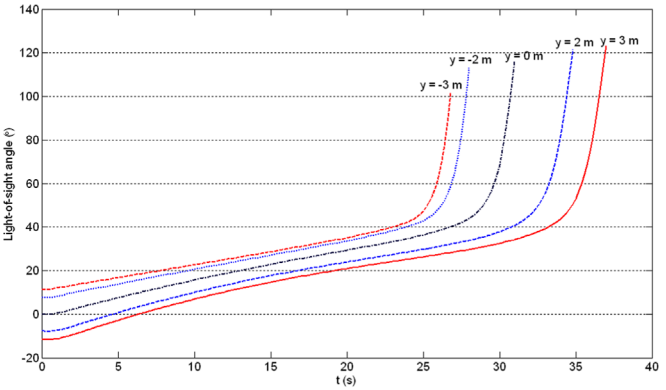

Fig. 17. Line-of-sight angle curve of proportional navigation guidance.

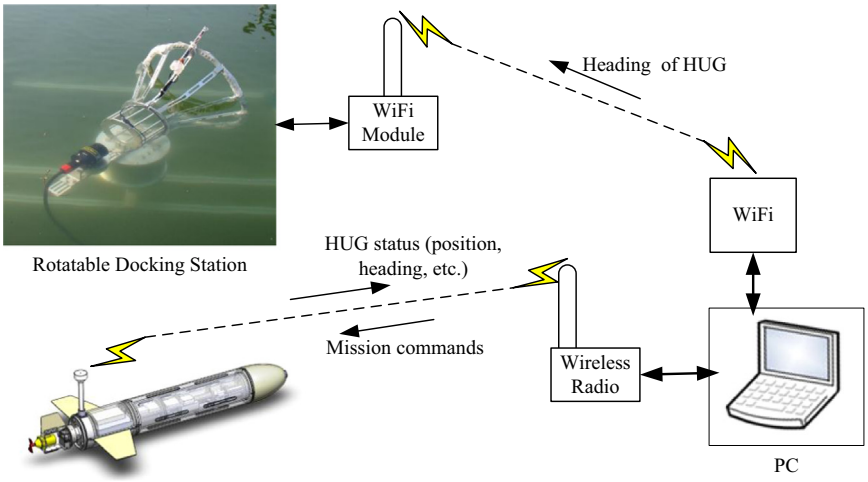

Fig. 18. Experimental system.

water initially. Besides, the acoustic devices for underwater communication and positioning were not available, which were still being debugged at the time we carried out the following experiments. Fortunately, there are other ways to solve this problem by locating the docking system on the water surface. The experimental docking system is setup as Fig. 18 shows. The dock station is located in the water with part of the dock entrance on the water surface. The control computer on the shore communicates with the dock station through WiFi. Since the vehicle sails on the water surface, it can receive the GPS signals for positioning; moreover, HUG can establish connection with the control computer using wireless communication terminals. Thus, both the positioning and attitude information of the vehicle can be sent to the control computer wirelessly in real time. The control computer then acts as a relay station transmitting such information to the dock station through WiFi. When the proximal docking stage begins, the dock station actuates the dock entrance to rotate according to the received information assisting the vehicle for a successful docking action.

During the test, when the range between the vehicle and dock is less than certain distance, the dock entrance starts to follow the vehicle's heading. At the same time, the vehicle approaches the funnel under the proposed guidance. Due to the wireless communication and the mechanical response, there may be some delay for the dock rotation. However, since the vehicle's speed is low and the range between the dock and the vehicle is long enough, the rotation of dock and the approach of vehicle can match up well.

5.2. Vision guidance system

In the docking system, a CCD (Charge Coupled Device) camera is mounted on the nose of the Mini-HUG vehicle, and an underwater lamp is installed on the dock. The image captured by the CCD camera is processed by an image processing board in the Electronic Section of Mini-HUG.

Through a serial of image process, such as object segmentation and extraction (Wang, 2014), the position of the underwater lamp in the image reference frame can be obtained, which is described in the unit pixels. Because only one underwater lamp is used for vision navigation, the distance between the dock and the approaching vehicle is not available. According to the method presented by Li et al. (2015), we can estimate the line-of-sight angle λ between the dock and the approaching vehicle, which can be used for vision navigation in docking process.

5.3. Experiment results

Fig. 19 presents the vehicle trajectories during the docking experiments with and without current disturbance. The current disturbance was made artificially by a water pump. As shown in Fig. 19, the black solid curve indicates the docking trajectory without current disturbance using pure pursuit guidance, the red dot curve shows the docking trajectory with current disturbance using pure pursuit guidance, and the blue dash dot curve represents the docking trajectory with current disturbance using pursuit guidance with current compensation. In the case of pure pursuit guidance without current disturbance, the vehicle can approach the dock entrance successfully. Comparing the trajectories with and without current disturbance, we can find that the cross currents caused remarkable cross-track and heading deviations to the vehicle. Since the pursuit guidance algorithm with current compensation compensated the current effect well, there was no big discrepancy between the black solid curve and the blue dashed dot curve at the docking entrance in Fig. 19. Besides, the rotatable dock entrance can follow the vehicle's heading actively ensuring the successes of these two docking attempts as well. As for the case of pure pursuit guidance under current disturbance

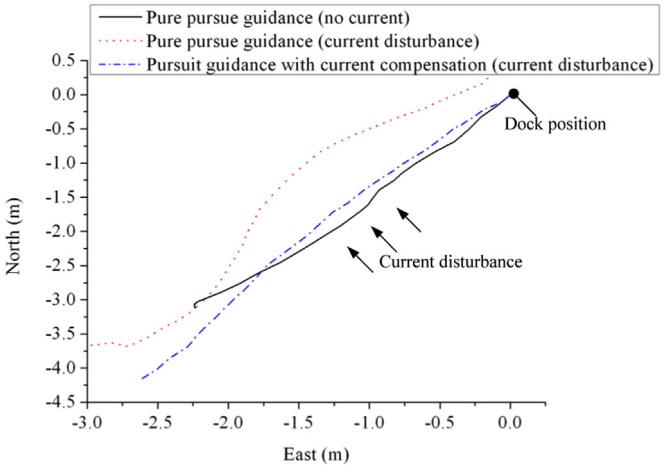

Fig. 19. Docking trajectories of HUG during the experiments. (For interpretation of the references to color in this figure legend, the reader is referred to the web version of this article.)

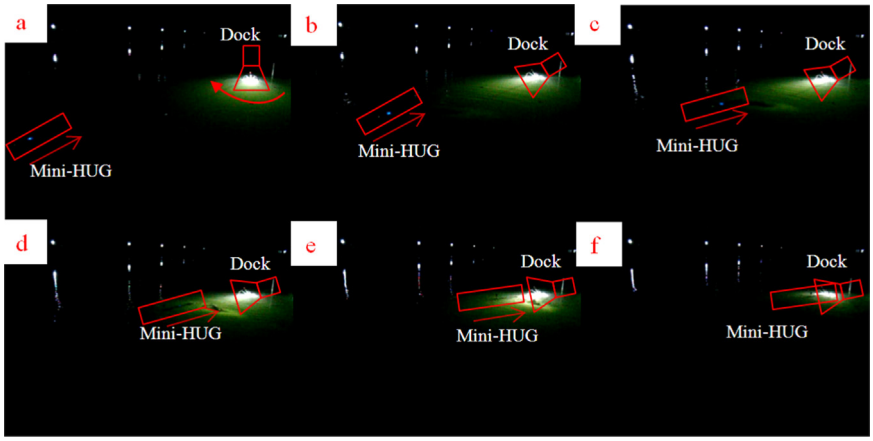

Fig. 20. Time-series photos for one docking attempt. The rectangle represents the location of the HUG; the straight arrow shows the motion trend of HUG; while the curved arrow indicates the rotation direction of the dock entrance.

but without current compensation, the current affected the vehicle motion a lot, and caused the failure of this docking attempt; see the red dot curve in Fig. 19.

To ensure the performance of vision navigation, the experiments were carried out in the dark, which simulated the light condition underwater. Fig. 20 shows the time-series photos for one docking attempt. It can be found that the dock rotated corresponding to the vehicle actively in real time, and then the vehicle entered the dock easily.

6. Conclusions

Since ocean currents bring serious disturbances on underwater docking operation, especially for underactuated vehicles, this paper presents a hybrid underwater glider with a rotatable thruster, which ensures the enough maneuverability of the vehicle for underwater docking. The high maneuverability of the vehicle has been validated by turning tests. Besides, a novel kind of docking scheme with a rotatable dock entrance is proposed, which can rotate actively to follow up the vehicle and increase the probability of successful docking.

Considering both the influence of the ocean currents and the view range of the sensors, such as USBL and camera, a pursuit guidance algorithm with current compensation is presented. The performance of the proposed algorithm is compared with the existing ones, including the pure pursuit and the proportional navigation guidance algorithms by simulation. The simulation results indicates that the proposed guidance algorithm compensates the current effects on the vehicle motion well, and maintains the dock in the views of the USBL and camera on the vehicle.

In addition, a series of experiments have been conducted to validate the proposed guidance algorithm preliminarily in the swimming pool. During the experiments, HUG using the proposed guidance algorithm entered the rotatable dock entrance successfully for several docking attempts under current disturbance, which demonstrated the feasibility of the docking system and the effectiveness of the guidance algorithm proposed. Our ongoing research is focused on the complete docking system development with acoustic devices for underwater communication and positioning, and the field trials will be carried out to verify the robustness and stability of the docking system.

Acknowledgment

The authors gratefully acknowledge the financial support by the Science Fund for Creative Research Groups of National Natural Science Foundation of China (No. 51521064), the program for Zhejiang Leading Team of S&T Innovation (Grant No. 2010R50036), China Postdoctoral Science Foundation (No. 2015M571869) and “Electronic Science and technology” Zhejiang Open Foundation of the Most Important Subjects. The authors also appreciate the helpful feedback from the anonymous reviewers.

References

Allen, B., Austin, T., Forrester, N., Goldsborough, R., Kukulya, A., 2006. Autonomous docking demonstrations with enhanced REMUS technology. In: OCEANS 2006, Vol. 1–4, IEEE, New York, pp. 1539–1544.

Alvarez, A., Caffaz, A., Caiti, A., Casalino, G., Gualdesi, L., Turetta, A., Viviani, R., 2009. Folaga: a low-cost autonomous underwater vehicle combining glider and AUV capabilities. Ocean Eng. 36 (1), 24–38.

Bachmayer, R., Leonard, N.E., Graver, J., Fiorelli, E., Bhatta, P., Paley, D., 2004. Underwater gliders: Recent developments and future applications. In: Proceedings of the 4th International Symposium on Underwater Technology, IEEE, Taibei, pp. 195–200.

Caffaz, A., Caiti, A., Casalino, G., Turetta, A., 2010. The hybrid glider/AUV Folaga field experience at the GLINT'08 experiment. IEEE Robot. Autom. Mag. 17 (1), 31–44.

Chen, Y., Yang, C., Li, D., Jin, B., Chen, Y., 2012a. Design and application of a junction box for cabled ocean observatories system. Mar. Technol. Soc. J. 46 (3), 50–63.

Chen, Y., Yang, C., Li, D., Jin, B., Chen, Y., 2012b. Study of a DC power system for a multi-node cabled ocean observatories system. J. Zhejiang Univ. Sci. C 13 (8), 613–623.

Chen, Y., Yang, C., Li, D., Jin, B., Chen, Y., 2013. Study on 10 kV DC powered junction box for cabled ocean observatory system. China Ocean Eng. 27 (2), 265–275.

Claus, B., Bachmayer, R., Cooney, L., 2012. Analysis and development of a buoyancy-pitch based depth control algorithm for a hybrid underwater glider. In: Proceedings of the 2012 IEEE/OES Autonomous Underwater Vehicles (AUV). IEEE, Southampton, pp. 1–6.

Claus, B., Bachmayer, R., Williams, C.D., 2010. Development of an auxiliary propulsion module for an autonomous underwater glider. Proc. Inst. Mech. Eng. Part M: J. Eng. Marit. Environ. 224 (4), 255–266.

Cottrell, R.G., 1971. Optimal intercept guidance for short-range tactical missiles. AIAA J. 9 (7), 1414–1415.

Crosswind landing, 2009. Retrieved 2015-3-29 from ⟨https://en.wikipedia.org/wiki/Crosswind_landing⟩.

Fan, S., Woolsey, C.A., 2014. Dynamics of underwater gliders in currents. Ocean Eng. 84, 249–258.

Feitian, Z., Thon, J., Thon, C., Xiaobo, T., 2014. Miniature underwater glider: design and experimental results. IEEE/ASME Trans. Mechatron. 19 (1), 394–399.

Fossen, T.I., 1995. Guidance and Control of Ocean Vehicles. John Wiley and Sons, Inc, New York, USA, p. 162.

Graver, J.G., 2005. Underwater Gliders: Dynamics, Control and Design (Ph.D. thesis). Princeton University,, Princeton, New Jersey, U.S., p. 273.

Hu, B., Tian, H., Qian, J., Xie, G., Mo, L., Zhang, S., 2013. A Fuzzy-PID method to improve the depth control of AUV. In: Proceedings of the 2013 IEEE International Conference on Mechatronics and Automation. IEEE, pp. 1528–1533.

Isa, K., Arshad, M.R., 2013. Modeling and motion control of a hybrid-driven

underwater glider. Indian J. Geo-Mar. Sci. 42 (8), 971–979.
Isa, K., Arshad, M.R., Ishak, S., 2014. A hybrid-driven underwater glider model, hydrodynamics estimation, and an analysis of the motion control. Ocean Eng. 81 (2), 111–129.
Jenkins, S.A., Humphreys, D.E., Sherman, J., Osse, J., Jones, C., Leonard, N.E., Wasyl, J. 2003. Underwater glider system study. In: Technical report No. 53, Scripps Institution of Oceanography, San Diego, CA.
Kim, J., 2007. Dual Control Approach for Automatic Docking Using Monocular Vision (Ph.D. thesis). Stanford University, Stanford, California, U.S.
Li, B., Xu, Y., Liu, C., Fan, S., Xu, W., 2015. Terminal navigation and control for docking an underactuated autonomous underwater vehicle. In: Proceedings of the 2015 IEEE International Conference on Cyber Technology in Automation, Control, and Intelligent Systems (CYBER). IEEE, Shenyang, pp. 25–30.
Mahmoudian, N., 2009. Efficient Motion Planning and Control for Underwater Gliders (Ph.D. thesis). Virginia Polytechnic Institute and State University, Blacksburg, Virginia, U.S, p. 110.
Mahmoudian, N., Woolsey, C., 2008. Underwater glider motion control. In: Proceedings of the 47th IEEE Conference on Decision and Control. IEEE, Cancun, Mexico, pp. 552–557.
McEwen, R.S., Hobson, B.W., McBride, L., Bellingham, J.G., 2008. Docking control system for a 54-cm-diameter (21-in) AUV. IEEE J. Ocean. Eng. 33 (4), 550–562.
Morel, Y., 2002. Design of an Adaptive Nonlinear Controller for an Autonomous Underwater Vehicle Equipped With a Vectored Thruster (Master of Science thesis). Florida Atlantic University, Boca Raton, Florida, U.S.
Park, J., Jun, B., Lee, P., Lim, Y., Oh, J., 2011a. Modified linear terminal guidance for docking and a time-varying ocean current observer. In: Proceedings of the 2011 IEEE Symposium on Underwater Technology (UT) and 2011 Workshop on Scientific Use of Submarine Cables and Related Technologies (SSC). IEEE, Tokyo, pp. 1–6.
Park, J., Jun, B., Lee, P., Lim, Y., Oh, J., 2011b. Docking problem and guidance laws considering drift for an underactuated AUV. In: MTS/IEEE Oceans. IEEE, Spain, pp. 1–7.
Park, J., Jun, B., Lee, P., Oh, J., 2009. Experiments on vision guided docking of an autonomous underwater vehicle using one camera. Ocean Eng. 36 (1), 48–61.
Peng, S., Yang, C., Fan, S., Zhang, S., Wang, P., Chen, Y., 2014. Hybrid underwater glider for underwater docking: modeling and performance evaluation. Mar. Technol. Soc. J. 48 (6), 112–124.
Peng, S., Yang, C., Fan, S., Zhang, S., Wang, P., Xie, Y., Chen, Y., 2013. A hybrid underwater glider for underwater docking. In: MTS/IEEE Oceans. IEEE, San Diego, California, pp. 1–7.
Ryoo, C., Cho, H., Tahk, M., 2006. Time-to-go weighted optimal guidance with impact angle constraints. IEEE Trans. Control Syst. Technol. 14 (3), 483–492.
Shaferman, V., Shima, T., 2008. Linear quadratic guidance laws for imposing a terminal intercept angle. J. Guid. Control Dyn. 31 (5), 1400–1412.
Shi, J., Zhang, S., Yang, C., 2012. High frequency RF based non-contact underwater communication. In: MTS/IEEE Oceans. IEEE, Yeosu, Korea, pp. 1–6.
Singh, H., Bellingham, J.G., Hover, F., Lemer, S., Moran, B.A., von der Heydt, K., Yoerger, D., 2001. Docking for an autonomous ocean sampling network. IEEE J. Ocean. Eng. 26 (4), 498–514.
Steinfeldt, B.A., Grant, M.J., Matz, D.A., Braun, R.D., Barton, G.H., 2010. Guidance, navigation, and control system performance trades for Mars pinpoint landing. J. Spacecr. Rockets 47 (1), 188–198.
Tan, X., 2011. Autonomous robotic fish as mobile sensor platforms: challenges and potential solutions. Mar. Technol. Soc. J. 45 (4), 31–40.
Teo, K., An, E., Beaujean, P., 2012. A robust fuzzy autonomous underwater vehicle (AUV) docking approach for unknown current disturbances. IEEE J. Ocean. Eng. 37 (2), 143–155.
Teo, K., Goh, B., Chai, O.K., 2015. Fuzzy docking guidance using augmented navigation system on an AUV. IEEE J. Ocean. Eng. 40 (2), 349–361.
Thivierge, D.P., Dooley, R.E., Menozzi, A., Treaster, A.L., Beam, M.J., Fetterolf, T.K., Metrey, D.R., 2005. Articulation Mechanism and elastomeric Nozzle for Thrust-vectored Control of an Undersea Vehicle. US7465201 B1.
Wang, H., 2014. Study of Robot Vision Navigation System for Deep Sea Docking (Master thesis). Zhejiang University, Hangzhou, Zhejiang Province, China.
Wang, S.X., Sun, X.J., Wang, Y.H., Wu, J.G., Wang, X.M., 2011. Dynamic modeling and motion simulation for a winged hybrid-driven underwater glider. China Ocean Eng. 25 (1), 97–112.
Wang, S.X., Sun, X.J., Wu, J.G., Wang, X.M., Zhang, H.W., 2010. Motion characteristic analysis of a hybrid-driven underwater glider. In: MTS/IEEE Oceans. IEEE, Sydney, Australia.
Watson, S.A., Green, P.N., 2014. Depth control for micro-autonomous underwater vehicles (μAUVs): simulation and experimentation. Int. J. Adv. Robot. Syst. 31 (11), 1–10.
Woolsey, C.A., 2005. Reduced Hamiltonian dynamics for a rigid body/mass particle system. J. Guid. Control Dyn. 28 (1), 131–138.
Woolsey, C.A., 2011. Vehicle Dynamics in Currents. Virginia Polytechnic Institute and State University, Blacksburg.
Xu, X., Liang, Y., 2015. Biased optimal guidance law with specified velocity rendezvous angle constraint. Aeronaut. J. 119 (1220), 1287–1299.
Zhang, F., Zhang, F., Tan, X., 2012. Steady spiraling Motion of gliding Robotic Fish. In: Proceedings of the 2012 IEEE/RSJ International Conference on Intelligent Robots and Systems, IEEE, Vilamoura, Algarve, Portugal, pp. 1754–1759.